Abstract
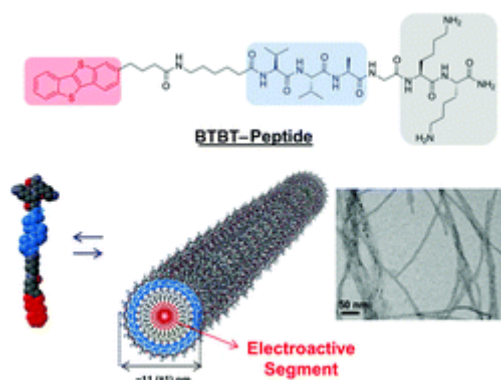
π-Conjugated small molecules based on a [1]benzothieno[3,2-*b*]benzothiophene (BTBT) unit are of great research interest in the development of solution-processable semiconducting materials owing to their excellent charge-transport characteristics. However, the BTBT π-core has yet to be demonstrated in the form of electro-active one-dimensional (1D) nanowires that are self-assembled in aqueous media for potential use in bioelectronics and tissue engineering. Here we report the design, synthesis, and self-assembly of benzothienobenzothiophene (BTBT)–peptide conjugates, the **BTBT–peptide** (BTBT-C$_3$–COHN-Ahx-VVAGKK-Am) and the **C$_8$-BTBT–peptide** (C$_8$-BTBT-C$_3$–COHN-Ahx-VVAGKK-Am), as β-sheet forming amphiphilic molecules, which self-assemble into highly uniform nanofibers in water with diameters of 11–13(±1) nm and micron-size lengths. Spectroscopic characterization studies demonstrate the J-type π–π interactions among the BTBT molecules within the hydrophobic core of the self-assembled nanofibers yielding an electrical conductivity as high as 6.0×10^{-6} S cm^{-1}. The BTBT π-core is demonstrated, for the first time, in the formation of self-assembled peptide 1D nanostructures in aqueous media for potential use in tissue engineering, bioelectronics and (opto)electronics. The conductivity achieved here is one of the highest reported to date in a non-doped state.

Introduction

π-Conjugated small molecules based on [1]benzothieno[3,2-*b*]benzothiophene (BTBT) have attracted enormous interest in the solution-processable organic semiconductor field owing to their record high-performances in organic field-effect transistors (OFETs)[1,2] and use in relevant (opto)electronic applications such as photovoltaic devices and flexible displays.[3–6] Since the first report of a BTBT-based semiconductor in 2006 by Takimiya *et al.*,[7] impressive high hole mobilities up to 43 cm^2 V^{-1} s^{-1} have been achieved in OFET devices when these p-type semiconductors are solution-processed (*e.g.*, spin-coated, gravure-printed, drop-casted, *etc.*) from organic solvents into thin-films.[8] Compared to most of the previously developed π-conjugated structures, the BTBT π-core offers superior structural and electronic properties such as good solubility in organic solvents, high-crystallinity, co-planarity, facile synthesis and structural functionalization, and efficient charge-transport, which overall make this π-core quite attractive for further applications in tissue engineering and bioelectronics. However, the BTBT π-core has yet to be demonstrated in the form of electroactive self-assembled one-dimensional (1D) nanowires in aqueous media for potential use in bioelectronics and tissue engineering. The biomolecular self-assembly has been an attractive tool over the past few decades to prepare a variety of well-defined supramolecular nanostructures such as micelles, sheets, vesicles, tubes, and fibers.[9–12] Peptide-based

supramolecular nanostructures are particularly of great interest due to their biocompatibility, biofunctionality, stimuli responsiveness, and rich functionality.[13,14] As a result of the structural versatility and facile synthesis, numerous peptide-based supramolecular nanostructures with various chemical compositions have previously been developed and extensively studied for tissue engineering, drug delivery, sensing, catalysis, optoelectronic and biomedical applications.[14–16] Recently, there is also a growing research interest to employ a semiconductor-peptide-based self-assembly process in the bottom-up fabrication of supramolecular nanostructured (opto)electronic materials.[14,17] In a typical approach, a π-conjugated organic (semi)conductor small molecule is covalently attached to a short self-assembling peptide sequence, and these peptidic organic π-structure amphiphiles self-assemble into well-defined 1D nanostructures under aqueous conditions. This type of electroactive nanostructures formed in aqueous media hold great promise in a variety of applications in (opto)electronics, organic chromophore arrays and bioelectronics.[17,18] Several research groups have previously reported that self-assembling peptide sequences having π-conjugated semiconducting structures can form 1D nanowires. However, only a limited number of π-conjugated systems such as oligothiophene, naphthalenediimide, pyrene, and oligo(p-phenylenevinylene) were used in these studies.[17,19,20] Therefore, it is still very important to further investigate new semiconductor structures, especially the high-performing ones prepared by the peptide self-assembly process to widen the scope of biocompatible (opto)electronic materials. Therefore, we envision that the self-assembled nanostructures formed in aqueous media from **BTBT–peptide**conjugates, which employ charge-transporting BTBT π-units in the hydrophobic core, may pave the way to various applications in bioelectronics and tissue engineering. On the other hand, developing a widely applicable synthetic approach to covalently link π-conjugated cores and peptide sequences, without requiring any specific functional group on the semiconductor π-system, would enable further development of novel semiconductor-peptide nanostructures in this field.

Here we report the design, synthesis, and self-assembly of β-sheet forming semiconductor–peptide amphiphilic molecules, the **BTBT–peptide** (BTBT-C$_3$–COHN-Ahx-VVAGKK-Am) and the **C$_8$-BTBT–peptide** (C$_8$-BTBT-C$_3$–COHN-Ahx-VVAGKK-Am), in aqueous media, which assemble into highly uniform nanofibers with a diameter of 11–13(±1) nm and a micron-size length as evidenced by atomic force microscopy (AFM) and transmission electron microscopy (TEM) (Fig. 1). The self-assembly process and the photophysical properties of the corresponding nanofibers are studied, which indicates the formation of the J-aggregated BTBT π-cores with extended π-delocalizations in the hydrophobic core. The hydrophobicity of the π-system (BTBT $vs.$ C$_8$-BTBT) is found to have a profound effect on the self-assembly process. The charge transport characteristics were measured for the nanofiber-based peptide films by depositing Au electrodes via thermal evaporation, which yielded an electrical conductivity of 4.2(±1.8) × 10^{-6} S cm^{-1} and 2.4(±0.47) × 10^{-7} S cm^{-1} for the **BTBT–peptide**and the **C8-BTBT–peptide**, respectively. The synthetic method employed here to functionalize the BTBT π-core for covalent attachment to the peptide sequence is a two-step approach, which does not require any pre-existing functional group on the π-system, and it should be broadly applicable to other π-conjugated organic semiconductors. Herein, the BTBT π-core is demonstrated, for the first time, in the form of an electroactive self-assembled peptide nanostructure in aqueous media for potential use in tissue engineering and bioelectronics applications. The electrical conductivity measured herein is among the highest reported to date for a non-doped peptide film.
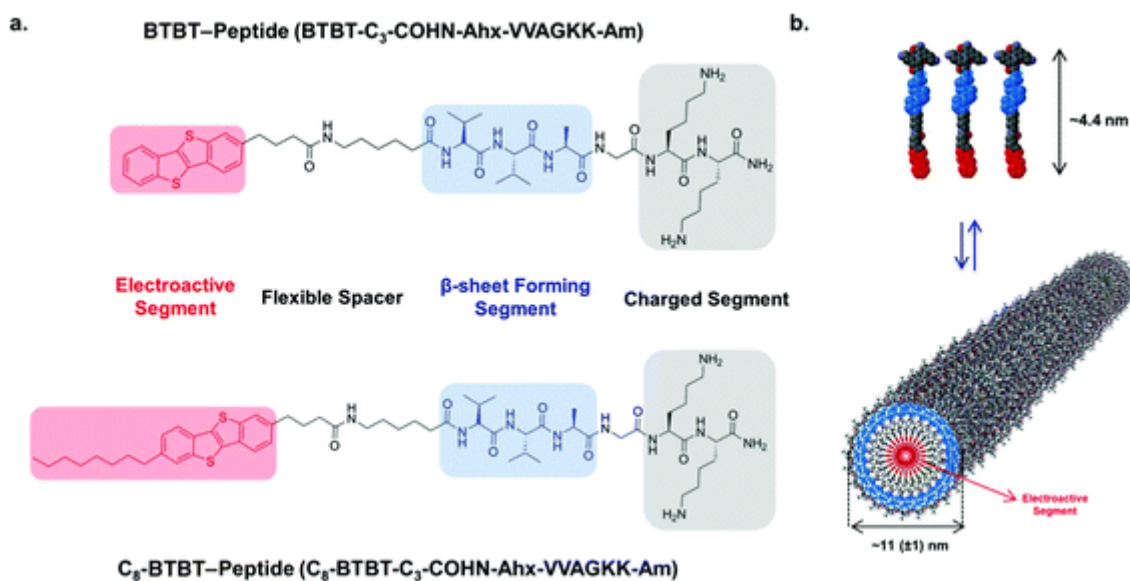
1 (a) Molecular structures of the [1]benzothieno [3,2-*b*] benzothiophene (BTBT)–peptide amphiphiles, the **BTBT–peptide** (BTBT–C_3-COHN-Ahx-VVAGKK-Am) and the **C_8-BTBT–peptide** (C_8-BTBT–C_3-COHN-Ahx-VVAGKK-Am). (b) A schematic presentation of the self-assembly process for the **BTBT–peptide** amphiphile showing the proposed nanofiber structure with the computed molecular length (~4.4 nm) and the measured nanofiber diameter (~11 ± 1 nm).

Results and discussion

Synthesis of BTBT molecules

The rational design of the new BTBT precursors for peptide attachment is based on the fact that the electronic structure of the [1]benzothieno[3,2-*b*]benzothiophene (BTBT) π-core should not be altered while becoming structurally compatible with a solid phase peptide synthesis (SPPS) technique. Therefore, we have designed and synthesized two precursors with (2-[1]benzothieno[3,2-*b*][1]benzothiophenebutyric acid (**BTBT-C_3-COOH**)) and with (7-octyl-2-[1]benzothieno[3,2-*b*][1]benzothiophenebutyric acid (**C_8-BTBT-C_3-COOH**)) a linear alkyl chain (*n*-C_8H_{17}) at BTBT's 7-position (Scheme 1). Both derivatives are functionalized with butyric acid (–C_3H_6COOH) at BTBT's 2-position to enable covalent attachment to the peptide. The terminal carboxylic acid groups provide the required functionality to react with the peptide amino (–NH_2) group in the solid phase peptide synthesis (SPPS). In this design, a linear propylene (C_3) spacer was placed between the carboxylic functional group and the BTBT π-core to eliminate any inductive or mesomeric effects of the electron-withdrawing –COOH group and also to provide structural flexibility (increased degrees of freedom) to the BTBT π-core to adapt the optimal packing in the 1-D nanostructured channel. In the semiconductor–peptide conjugates, **BTBT–peptide** (BTBT–C_3-COHN-Ahx-VVAGKK-Am) and **C_8-BTBT–peptide** (C_8-BTBT-C_3-COHN-Ahx-VVAGKK-Am), **BTBT-C_3-COOH** and **C_8-BTBT-C_3-COOH** molecules are covalently conjugated to a hexapeptide sequence (H_2N-Ahx-VVAGKK-Am) (Fig. 1). In this molecular design, while the VVA sequence promotes the formation of β-sheets assisting aggregation, the two lysine (KK) amino acids provide positively charged sites, ensuring good solubility in aqueous media.[21]
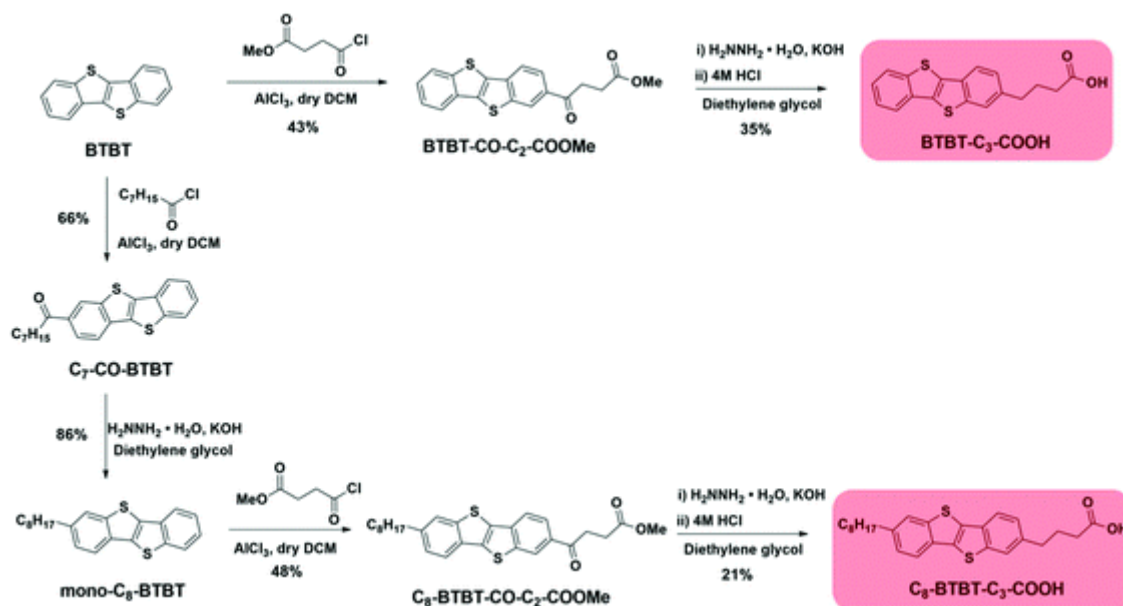
Scheme 1 Synthetic routes to **BTBT-C₃-COOH** and **C₈-BTBT-C₃-COOH**.

On the other hand, the BTBT π-core serves as both electroactive and hydrophobic segment to derive the hydrophobic collapse of semiconductor−peptide amphiphiles in aqueous media forming 1D nanowires. In addition to the propylene spacer in the BTBT precursor, a six carbon spacer (Ahx) was introduced between the BTBT amide group and the hexapeptide sequence to allow the semiconducting BTBT molecules to be organized in a favorable supramolecular conformation during the self-assembly process. The synthetic routes to **BTBT-C₃-COOH** and **C8-BTBT-C₃-COOH** are shown in Scheme 1 and the experimental procedures are provided in the Experimental section. The synthesis of **BTBT-C₃-COOH** was performed in two steps. BTBT first undergoes a Friedel–Crafts acylation reaction with methyl 4-chloro-4-oxobutyrate in the presence of an AlCl₃ Lewis catalyst to yield methyl 2-[1]benzothieno[3,2-*b*][1]benzothiophenebutyrate (**BTBT-CO-C₂-COOMe**) in 43% yield. Note that this reaction is a selective acylation with the acyl chloride functionality and the methyl ester group in the reagent remains unreacted. Since carbonyl (–CO–) is a well-known electron-withdrawing functionality and can significantly change the electronic structure of BTBT (*i.e.*, π-electron-density, HOMO/LUMO energies, band gap, and charge-transport behavior), in the second step, the carbonyl group (–CO–) which is directly attached to the phenyl ring of the BTBT π-core is converted to methylene (–CH₂–) *via* the Wolf–Kishner reduction reaction in the presence of NH₂NH₂/KOH in diethylene glycol. This reaction condition provides a strongly basic medium to simultaneously enable the hydrolysis of the methyl ester to a carboxylate group, which upon acidification yields **BTBT-C₃-COOH** in 35% yield. The same two-step approach was also employed starting with octyl-substituted BTBT (**mono-C₈-BTBT**) in the synthesis of **C₈-BTBT-C₃-COOH**. Note that **mono-C₈-BTBT** was prepared *via* the Friedel–Crafts acylation of unsubstituted BTBT with octanoyl chloride and a subsequent Wolf–Kishner reduction in 57% total yield. The intermediate compounds and the final BTBT-based carboxylic acid containing precursors were purified by silica gel column chromatography, and the chemical structures and the purities were evaluated using ¹H/¹³C NMR (Fig. S1 and S2†), mass spectrometry (ESI) and thin-layer chromatography.

Synthesis of BTBT–peptide molecules

BTBT−peptide conjugates were synthesized using the solid phase peptide synthesis (SPPS) method. The synthesis was performed on MBHA Rink Amide resin by reacting

fluorenylmethyloxycarbonyl (Fmoc)-protected amino acids (2.0 equiv.), *O*-benzotriazole-*N,N,N′,N′*-tetramethyl-uronium-hexafluoro-phosphate (HBTU) (1.95 equiv.) and *N,N*-diisopropylethylamine (DIEA) (3.0 equiv.) for 6 h in each coupling step. Note that in the final steps of **BTBT–peptide** and the **C₈-BTBT–peptide** synthesis, 1.5 equivalents of **BTBT-C₃-COOH** and **C8-BTBT-C3-COOH** were added, respectively, and the coupling reactions were performed for an additional 24 h. Then, the protecting groups were removed and the BTBT–peptides were cleaved from the solid resin by a mixture of trifluoroacetic acid/triisopropylsilane/water. The **BTBT–peptide** products were precipitated into cold ether. The final products were collected as a white powder after centrifugation and lyophilization. The final **BTBT–peptide**amphiphile molecules were purified by preparative high performance liquid chromatography (prep-HPLC) and characterized by liquid chromatography-mass spectrometry (LC-MS) (Fig. S3 and S4†).

Self-assembly of BTBT–peptide molecules

UV-vis, fluorescence, circular dichroism (CD) and X-ray photoelectron spectroscopies (XPS) were conducted to study the self-assembly of the **BTBT–peptide** under different pH conditions. The absorption of the reference semiconductor C8-BTBT molecule in tetrahydrofuran (THF) and the **BTBT–peptide** molecule dissolved at pH = 2 showed the same spectra with well-resolved vibronic peaks at 275–350 nm, which can be attributed to π–π^* ($S_0 \rightarrow S_1$) electronic transition of the BTBT core (Fig. 2a). However, upon charge neutralization by increasing pH to 10, we observed a significant decrease in absorption intensity and a corresponding broadening along with a ~20 nm red-shift (Fig. 2a). Meanwhile, the emission profile of the **BTBT–peptide** at pH = 10 demonstrated also a broadening and significant red-shift ($\lambda_{em} = 350$ nm $\rightarrow 405$ nm) in the emission signal (Fig. 2b). The drastic changes in both UV-vis and fluorescence spectra switching from acidic (pH = 2) to basic (pH = 10) media revealed the presence of J-type π–π interactions among the BTBT molecules.[22] The observed excitonic behavior for the current self-assembled **BTBT–peptide** molecule is quite different from those of the previously reported vapor-deposited/spin-coated BTBT thin-films, which indicates that a different intermolecular arrangement and packing is achieved within these 1D nanofibers.[3,23]
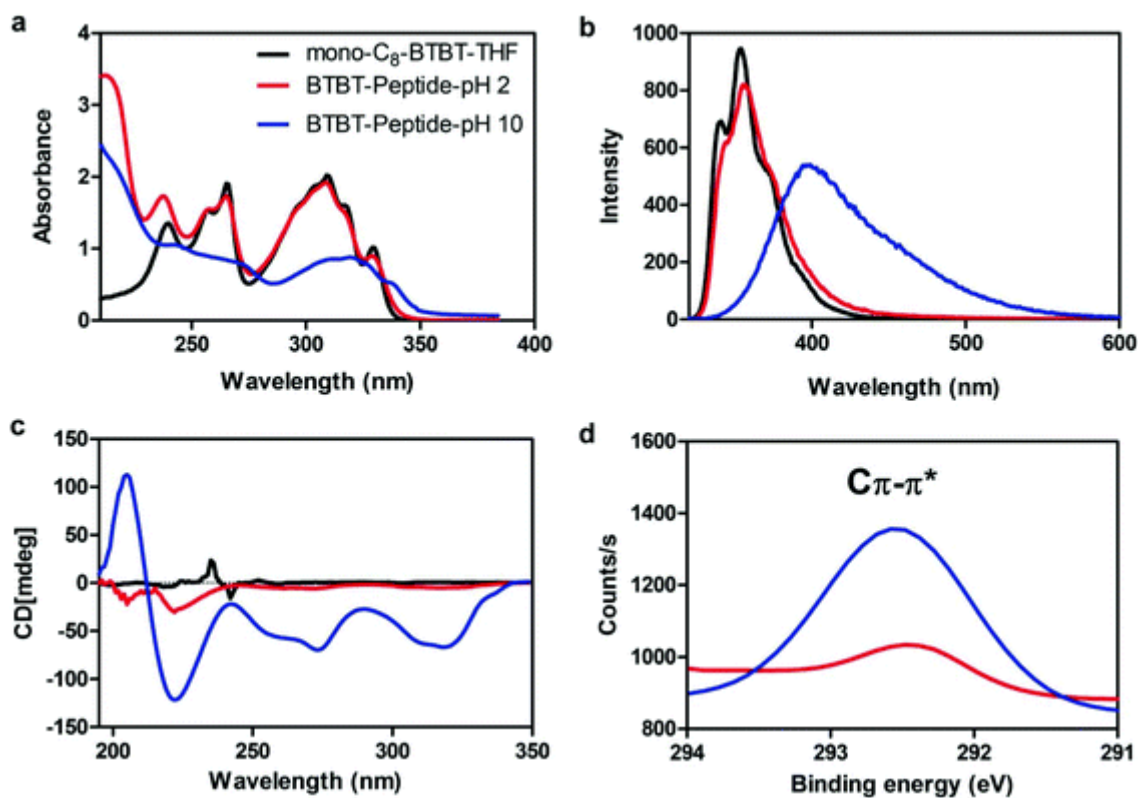
Fig. 2 Spectroscopic characterization of the **BTBT–peptide** self-assembly under different pH conditions. (a) UV-vis absorption, (b) fluorescence emission spectra (λ_{ex} = 310 nm) and (c) CD spectrum. (d) The XPS spectrum of C 1s for **BTBT–peptide** films prepared at pH = 2 and pH = 10.

Charge repulsions due to protonated amine groups in acidic media (pH = 2) prevent the proper aggregation of the **BTBT–peptide** molecules, and as a result, we did not observe CD signals (Fig. 2c). When the pH of the solution was adjusted to 10, several CD signals appeared. The negative cotton effect at 200–240 nm reveals the formation of highly ordered β-sheet secondary structures among the **BTBT–peptide** molecules (Fig. 2c).[24] Several other chiral signals were also observed at 240–350 nm, which confirms the induction of chirality in achiral BTBT molecules during self-assembly at pH = 10. The XPS analysis of C 1s of the **BTBT–peptide** film prepared at pH = 2 showed peaks corresponding to C–C, C–N and N–C=O bonds at 282–290 eV. A relatively weaker feature at 292.4 eV was also observed, which is found to increase notably along with a slight shift to higher energy (292.6 eV) upon self-assembly at pH = 10 (Fig. 2d). This feature is typically considered to be characteristic of aromatic compounds (π–π* transitions) and indicates the presence of the BTBT π-core.[25,26] Since BTBT is a small molecule π-system, the observed intensity increase and slight shift could be attributed to the intermolecularly delocalized π-system in the self-assembled BTBT as a result of molecular stacking in the hydrophobic core.

Imaging and scattering of BTBT–peptide nanofibers

Positively stained self-assembled **BTBT–peptide** nanofibers were imaged by transmission electron microscopy (TEM) showing the formation of well-defined 1D nanofibers with diameters of 11 ± 1 nm and micron-sized lengths (Fig. 3a and b), which was further confirmed by atomic force microscopy (AFM) (Fig. 3c and d). The SAXS data are shown in Fig. S5.† A core–shell cylinder model was employed to fit the data, using the software SASfit.[27] For the **BTBT–peptide**, the core radius is (2.18 ± 1.00) nm and the shell radius is 0.92 nm, giving a total fibril radius of (3.10 ±

1.00) nm. Considering that the **BTBT–peptide** is functionalized from only one side with a peptide sequence, the modeled molecular length in its fully extended conformation is estimated to be ~4.4 nm (Fig. S6†). Therefore, it is reasonable to propose that the nanofibers consist of circular alignments of the **BTBT–peptide** conjugates, which are somewhat overlapped/interdigitated in the hydrophobic core and aligned perpendicular to the fiber's long axis as modeled in Fig. 1b.
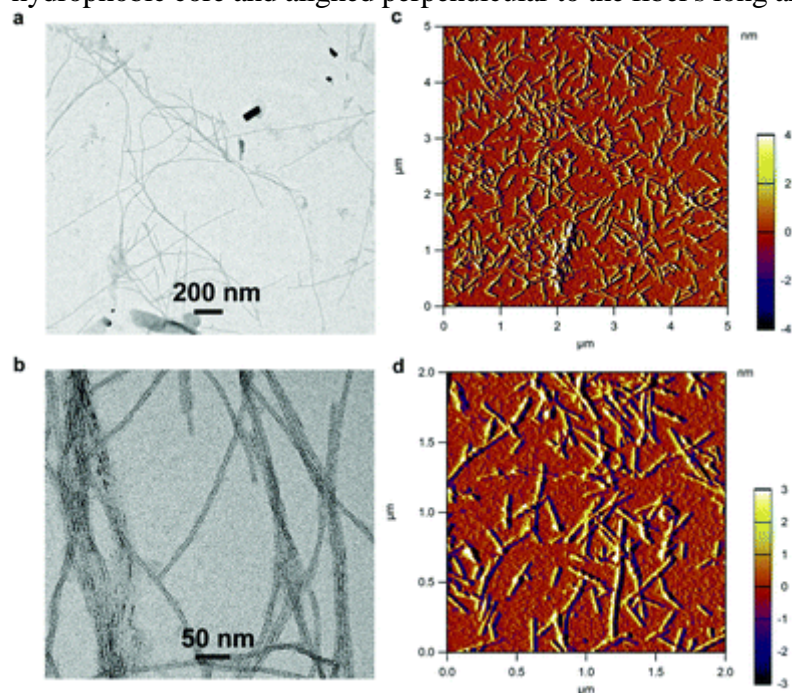

Fig. 3 Imaging of the **BTBT–peptide** molecule. TEM (a and b) and AFM images (c and d) of the **BTBT–peptide** nanofibers.

Self-assembly of C8-BTBT–peptide molecule

The self-assembly process for the **C$_8$-BTBT–peptide** molecule was also studied to observe how enhanced hydrophobicity affects aggregation behavior under different pH conditions. Compared to the **BTBT–peptide**, the **C$_8$-BTBT–peptide** includes a relatively more hydrophobic π-system since it contains a long lipophilic octyl (–C$_8$H$_{17}$) substituent at BTBT's 7-position. Interestingly, the **C$_8$-BTBT–peptide** molecule demonstrated a bathochromic shift ($\Delta\lambda_{onset} \approx 20$ nm) and a broadening of absorption bands in both acidic and basic media (Fig. 4a). Similarly, the emission maxima exhibited significant red shifts of ~60 nm ($\lambda_{em} = 350$ nm → 410 nm) under both acidic and basic conditions (Fig. 4b). These spectral changes reveal the existence of J-type π–π interactions between BTBT molecules at both high and low pH values.[22] Circular dichroism spectroscopy further confirms the self-assembly of the **C$_8$-BTBT–peptide** molecules in both acidic and basic media showing the presence of numerous chiral signals at both pH values of 2 and 10 (Fig. 4c).
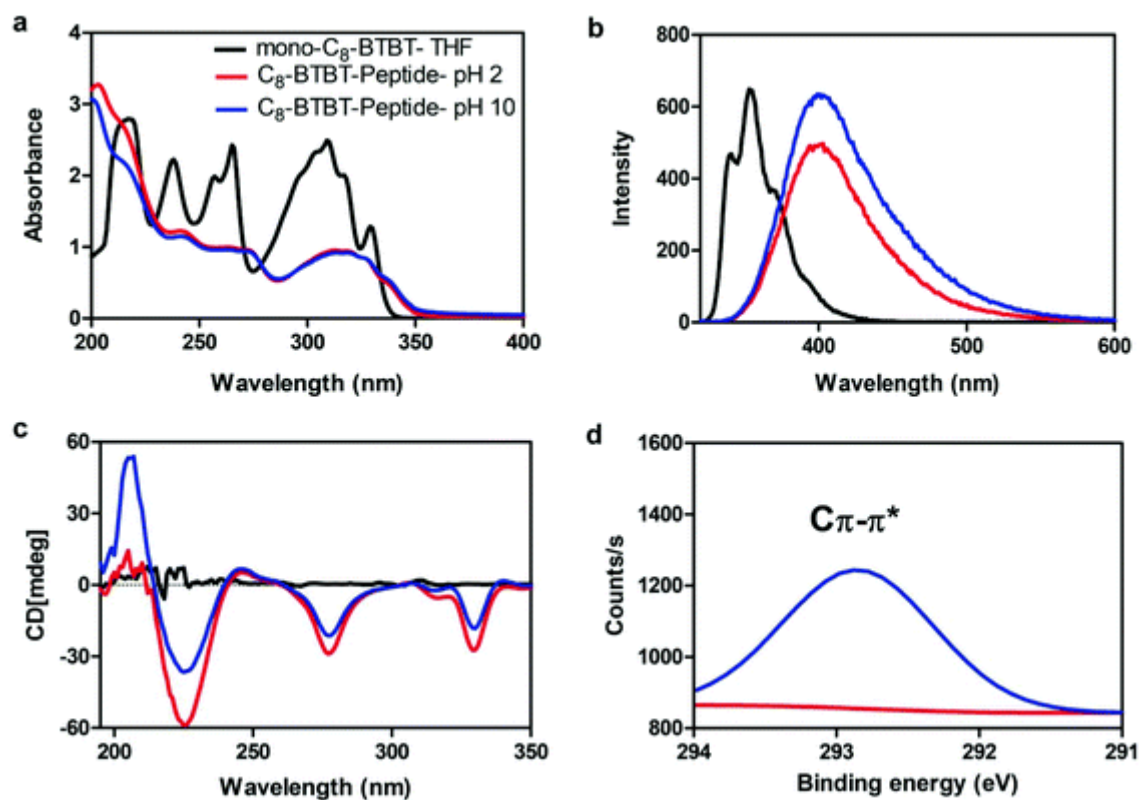
Fig. 4 Spectroscopic characterization of the **C8-BTBT–peptide** self-assembly under different pH conditions. (a) UV-vis absorption, (b) fluorescence emission spectra (λ_{ex} = 310 nm) and (c) CD spectrum. (d) XPS spectrum of C 1s for the **C8-BTBT–peptide** films prepared at pH = 2 and pH = 10.

While the **C8-BTBT–peptide** molecules shows β-sheet secondary structure formation in basic conditions (pH = 10) along with several other chiral signals, which are attributed to the absorption bands of the BTBT molecules, under a protonated condition (pH = 2), these signals are relatively less pronounced due to the presence of charge repulsion among the positively charged amine groups (Fig. 4c). Despite the presence of repulsive coulombic forces between the protonated amine groups at pH = 2, owing to the enhanced hydrophobic character of the **C8-BTBT–peptide**, hydrophobicity potentially dominates the coulombic repulsions to yield aggregation even in acidic media. The self-assembled **C8-BTBT–peptide** films prepared at pH = 10 showed a significantly enhanced π–π* shakeup feature at 292.8 eV, whereas the sample at pH = 2 did not show any peak in this range (Fig. 4d). This is attributed to the presence of an intermolecularly delocalized π-system in the self-assembled BTBT as a result of molecular stackings in the hydrophobic core.[25,26]

Imaging of C8-BTBT–peptide nanofibers

As shown by TEM, uranyl acetate stained C8-BTBT–peptide aggregates formed at basic pH exhibit well-defined 1D nanofibers with a diameter of 13 ± 1 nm and micron-sized length (Fig. 5a and b). As compared to the **BTBT–peptide**, the diameter increases by ∼1–2 nm for the **C8-BTBT–peptide** nanofibers, which agrees well with the computed molecular length increase from the **BTBT–peptide** (Fig. S6,† ∼4.4 nm) to the **C8-BTBT–peptide** (Fig. S6,† ∼5.4 nm), indicating that the substituent(s) on the BTBT π-core directly affect(s) the nanofiber diameter. Atomic force microscopy images further confirmed the presence of well-defined and micron-sized **C8-BTBT–peptide** nanofibers (Fig. 5c and d). Based on SAXS, the core radius was found to be (2.26 ± 1.00) nm, while the shell thickness is 1.48 nm, giving a total fiber radius of (3.74 ± 1.00) nm for the **C8-**

BTBT–peptide. As expected, this is larger than that of the **BTBT–peptide**. It is interesting that the shell radius is increased, but not the core radius. This suggests that, as far as SAXS contrast is concerned, some of the β-sheet peptide sequences form part of the shell in the fibrils. The small core radius indicates again that the folding or interdigitation of the hydrophobic end groups is even more pronounced than for the **BTBT–peptide**.
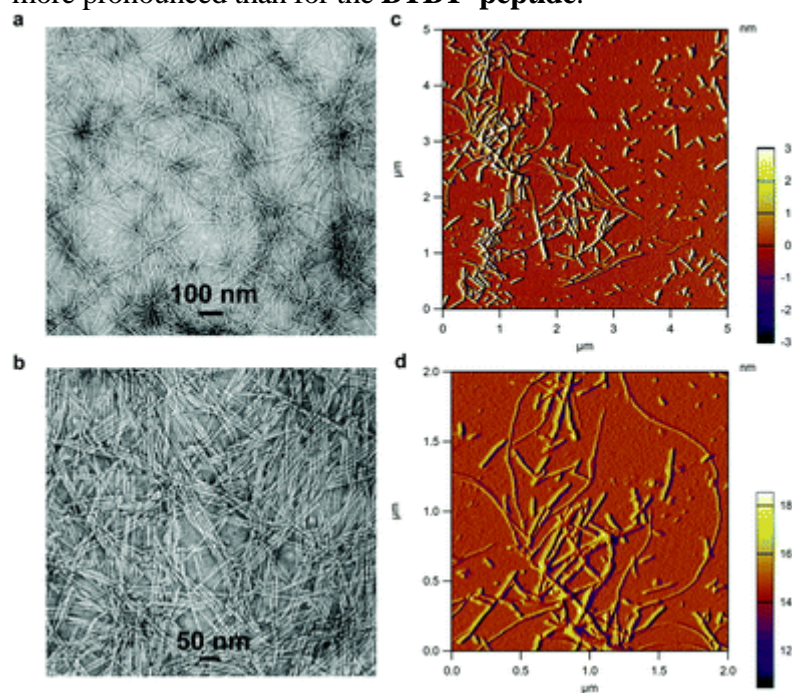
Fig. 5 Imaging of the **C$_8$-BTBT–peptide** molecule. TEM (a and b) and AFM (c and d) images of the C$_8$-BTBT-peptide nanofibers.

Electrical measurements of BTBT–peptide and C8-BTBT–peptide films

It is very important to measure the bulk conductivity of peptide nanofiber films since they can be used as 2D or 3D conductive scaffolds in tissue engineering applications.[28] Therefore, we performed electrical measurements on the peptide nanofiber films to study their charge-transport behavior. The 30 μL aqueous solutions of the **BTBT–peptide** or the **C$_8$-BTBT–peptide** samples were dropcast on a piranha solution-cleaned glass substrate (1.5 cm × 2 cm), which was then exposed to ammonia vapor in a sealed container for 20 min and dried overnight at 37 °C under vacuum. Au electrodes (50 nm thickness) were deposited through shadow masks using a thermal evaporation technique, which yielded conduction channels with 10–20 μm length and 1–4 mm width (Fig. 6a, b and Fig. S7–8†). The current–voltage characteristics of the resulting channels were measured under an ambient atmosphere by sweeping voltage between 0 and 20 V. The resulting current–voltage curve deviates from a linear trend, which is expected from an ideal resistor ($I = V/R$, where R is the resistance) (Fig. 6c and d). The nonlinear I–V curves are attributed to Schottky barrier formation between the electrodes and the films. The Schottky barriers could be present at the metal-(p-type) semiconductor junctions depending on the relative positions of the metal Fermi level and the highest occupied molecular orbital (HOMO) energy of the organic semiconductor. For the current semiconductor–peptide systems, since the HOMO energy level of the BTBT π-core is around −5.6 eV,[3] a certain degree of charge injection barrier could be expected for gold electrodes.[29] The Schottky contacts exhibit a rectifying behavior and behave like p–n diodes; thus the current–voltage relationship shows an exponential trend: $I = I_0(e^{V/nV_T} - 1)$, where I_0 is the reverse bias current, n is the ideality factor, and V_T is the thermal voltage (26 mV at room temperature). To extract the film resistance from the measured I–V curves, the Au-film junction is modeled as a diode and the film between the electrodes is modeled as a resistor (Fig.

S9†). In this case, the electrical conduction is limited by the diode owing to its rectifying behavior for small voltage levels, whereas it is limited by the resistor for higher voltage levels.
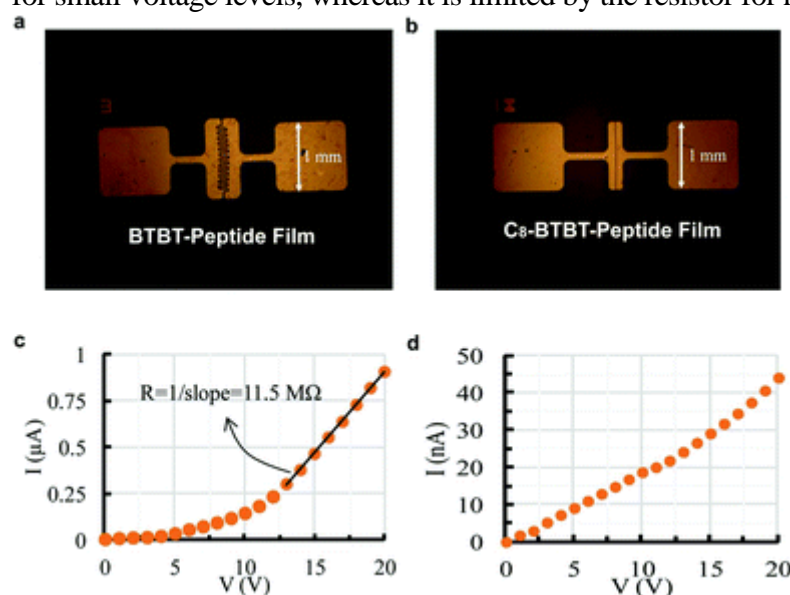
Fig. 6 Optical microscope images of Au contacts on the **BTBT–peptide** film with $L = 20$ μm and $W = 4$ mm (a) and the **C8-BTBT–peptide** film with $L = 10$ μm and $W = 1$ mm (b). *I–V* characteristics of the **BTBT–peptide** (c) and the **C8-BTBT–peptide** films between two Au electrodes (d).

The resistor-dominated voltage range is found by expressing the applied voltage as the sum of the voltage drops across the diode and the resistor, and taking the derivative of the total voltage with

$$V = V_D + V_R = nV_T \ln\left(\frac{I}{I_0} + 1\right) + IR \qquad \frac{dV}{dI} = \frac{nV_T}{I + I_0} + R$$

respect to the current:

The derivative of the total voltage with respect to the current shows a $1/I$ trend for low voltage levels and a constant value for increasing voltage levels revealing the resistance between the electrodes (Fig. S10†). Alternatively, the inverse of the slope for the linear fit to the *I–V* points in the resistor-dominated voltage range can be used to extract the resistance value (Fig. 6c). The effect of Schottky contacts is weaker for the **C8-BTBT–peptide** film suggesting that the electrical conduction is mostly resistor-dominated (Fig. 6d). The linear regions of the *I–V* curves are used to calculate the resistances for the **C8-BTBT–peptide** films as well.

The resistivity (ρ) and conductivity (σ) for the films are then calculated by accounting for the

$$\frac{1}{\sigma} = \rho = R\frac{t \times W}{L}.$$

channel length (*L*), width (*W*) and the film thickness (*t*) as follows:

The film thickness must be measured for each channel, since films exhibit large nonuniformity in thickness across the sample. The nonuniformity of the films is made evident by large variation in the resistance values (Table S1†). Atomic force microscopy is used for the thickness measurements (Fig. S11†). A step in the film is created by scribing the film for measurements. Table S1† shows the channel dimensions and the measured/calculated electrical properties of 7 devices from each sample. The average conductivity value for the **BTBT–peptide** film is calculated as $4.2(\pm 1.8) \times 10^{-6}$ S cm^{-1}, whereas the **C8-BTBT–peptide** film is found to be ~20 times more resistive with an average conductivity of $2.4(\pm 0.47) \times 10^{-7}$ S cm^{-1}. The decrease in conductivity for the **C8-BTBT–peptide** films as compared with the **BTBT–peptide** films could be attributed to the presence of octyl ($-C_8H_{17}$) chains attached to individual BTBT π-cores, which consist of a large number of insulating "C–C" and "C–H" σ-bonds. The presence of π-conjugated BTBT structures without insulating alkyl substituents in the hydrophobic channel of the **BTBT–peptide** film seems to induce more effective charge-transport behavior. Therefore, introducing different alkyl chains to

the **BTBT–peptide** molecules could be a facile strategy to fine tune the conductivity of the **BTBT–peptide** nanofibers. Until now, electroactive supramolecular self-assembled 1D nanostructures mainly suffer from low conductivity of 10^{-10}–10^{-9} S cm^{-1} in their non-doped states (Table S2†) and enhanced conductivities of 10^{-6}–10^{-4} S cm^{-1} were obtained only after p- or n-doping with oxidizing or reducing agents.[30–33] Remarkably, in the present study, we obtained a conductivity as high as 6.0×10^{-6} S cm^{-1} without using any doping agent, thanks to the rational design of the **C$_8$-BTBT–peptide** nanofibers, comprising an excellent p-type BTBT semiconductor. It is worth noting that the *I–V* curves achieved for the **BTBT–peptide** film using Al contacts are similar to what is observed with Au contacts (Fig. S12†). The mean conductivity value for the **BTBT–peptide** film with Al contacts is $2.6(\pm 0.9) \times 10^{-6}$ S cm^{-1}, which is within the range obtained for Au electrodes.

It is noteworthy that proteins and β-sheet assemblies have shown to be excellent proton conductors.[34–37] Due to the presence of rich hydrogen bonding, proton accepting and proton donating groups, proteins and the β-sheet fibrils may possibly assist effective proton conduction channels by the Grotthuss mechanism.[38] Therefore, we synthesized a control peptide molecule (Fig. S13–S15†), which does not contain any charge-transporting group, to investigate the contribution of proton conduction in **BTBT–peptide** nanofiber films. The control peptide molecule (KK) was revealed to form β-sheet structures and assemble into well-defined nanofibers in basic media, similar to **BTBT–peptide** conjugates.[21] The KK films were deposited on glass substrates and electrical measurements were conducted under similar conditions as in **BTBT–peptide** films. The conductivity results for KK films are summarized in Table S3† showing an average conductivity of 1.7×10^{-8} S cm^{-1} with a standard deviation of 0.6×10^{-8} S cm^{-1}. Therefore, it is clear that the **BTBT–peptide** films demonstrate a >200-fold enhancement in electrical conductivity as compared to the KK films measured under exactly the same conditions. The improvement in conductivity is attributed to the excellent charge-transporting π-system formed within these nanofibers by BTBT units.

Conclusion

In summary, we have developed a synthetic approach to functionalize a benchmark high-performance organic semiconductor, [1]benzothieno[3,2-*b*]benzothiophene (BTBT), to be compatible with the SPPS technique. Two derivatives of BTBT molecules were successfully conjugated to a β-sheet forming peptide with a positive charge. The **BTBT–peptide** molecules are readily soluble in aqueous media forming highly uniform nanofibers with a diameter of 11–13($\pm$1) nm and micron-size length. Spectroscopic characterization studies revealed the presence of J-type aggregations among the BTBT molecules resulting in extended π-delocalization within the hydrophobic part of the **BTBT–peptide** nanofibers. As a result, electrical measurements exhibited remarkable conductivities as high as 6.0×10^{-6} S cm^{-1} for **BTBT–peptide** films. The BTBT π-core has been demonstrated, for the first time, in the form of self-assembled peptide nanostructures in aqueous media for potential use in tissue engineering, (opto)electronics, and bioelectronics with one of the highest conductivity values achieved to date in a non-doped state.

Conflicts of interest

There are no conflicts to declare.

Acknowledgements

References

1. S. Fabiano , H. Usta , R. Forchheimer , X. Crispin , A. Facchetti and M. Berggren , *Adv. Mater.*, 2014, **26** , 7438 -7443 [CrossRef] [PubMed] .

2. M. Ozdemir , D. Choi , G. Kwon , Y. Zorlu , B. Cosut , H. Kim , A. Facchetti , C. Kim and H. Usta , *ACS Appl. Mater. Interfaces*, 2016, **8** , 14077 -14087 [Search PubMed] .

3. H. Ebata , T. Izawa , E. Miyazaki , K. Takimiya , M. Ikeda , H. Kuwabara and T. Yui , *J. Am. Chem. Soc.*, 2007, **129**, 15732 -15733 [CrossRef] [PubMed] .

4. V. Figa , C. Chiappara , F. Ferrante , M. P. Casaletto , F. Principato , S. Cataldo , Z. Chen , H. Usta , A. Facchettiand B. Pignataro , *J. Mater. Chem. C*, 2015, **3** , 5985 -5994 [RSC] .

5. R. Ozdemir , D. Choi , M. Ozdemir , G. Kwon , H. Kim , U. Sen , C. Kim and H. Usta , *J. Mater. Chem. C*, 2017, **5**, 2368 -2379 [RSC] .

6. K. Takimiya , S. Shinamura , I. Osaka and E. Miyazaki , *Adv. Mater.*, 2011, **23** , 4347 - 4370 [CrossRef] [PubMed] .

7. K. Takimiya , H. Ebata , K. Sakamoto , T. Izawa , T. Otsubo and Y. Kunugi , *J. Am. Chem. Soc.*, 2006, **128** , 12604 -12605 [CrossRef] [PubMed] .

8. Y. Yuan , G. Giri , A. L. Ayzner , A. P. Zoombelt , S. C. Mannsfeld , J. Chen , D. Nordlund , M. F. Toney , J. Huangand Z. Bao , *Nat. Commun.*, 2014, **5** , 3005 [Search PubMed] .

9. H. Gradiar and R. Jerala , *J. Nanobiotechnol.*, 2014, **12** , 4 [CrossRef] [PubMed] .

10. P. W. K. Rothemund *Nature*, 2006, **440** , 297 -302 [CrossRef] [PubMed] .

11. G. C. L. Wong , J. X. Tang , A. Lin , Y. L. Li , P. A. Janmey and C. R. Safinya , *Science*, 2000, **288** , 2035 -2039 [CrossRef] [PubMed] .

12. L. H. Yang , H. J. Liang , T. E. Angelini , J. Butler , R. Coridan , J. X. Tang and G. C. L. Wong , *Nat. Mater.*, 2004,**3** , 615 -619 [CrossRef] [PubMed] .

13. E. Arslan , I. C. Garip , G. Gulseren , A. B. Tekinay and M. O. Guler , *Adv. Healthcare Mater.*, 2014, **3** , 1357 -1376 [CrossRef] [PubMed] .

14. M. S. Ekiz , G. Cinar , M. A. Khalily and M. O. Guler , *Nanotechnology*, 2016, **27** , 402002 [CrossRef] [PubMed] .

15. H. Hosseinkhani , P. D. Hong and D. S. Yu , *Chem. Rev.*, 2013, **113** , 4837 - 4861 [CrossRef] [PubMed] .

16. G. Wei , Z. Su , N. P. Reynolds , P. Arosio , I. W. Hamley , E. Gazit and R. Mezzenga , *Chem. Soc. Rev.*, 2017, **46** , 4661 -4708 [RSC] .

17. J. D. Tovar *Acc. Chem. Res.*, 2013, **46** , 1527 -1537 [CrossRef] [PubMed] .

18. H. A. M. Ardona and J. D. Tovar , *Bioconjugate Chem.*, 2015, **26** , 2290 - 2302 [CrossRef] [PubMed] .

19. G. L. Eakins , R. Pandey , J. P. Wojciechowski , H. Y. Zheng , J. E. A. Webb , C. Valery , P. Thordarson , N. O. V. Plank , J. A. Gerrard and J. M. Hodgkiss , *Adv. Funct. Mater.*, 2015, **25** , 5640 -5649 [CrossRef] .

20. M. A. Khalily , G. Bakan , B. Kucukoz , A. E. Topal , A. Karatay , H. G. Yaglioglu , A. Dana and M. O. Guler , *ACS Nano*, 2017, **11** , 6881 -6892 [CrossRef] [PubMed] .

21. M. A. Khalily , M. Goktas and M. O. Guler , *Org. Biomol. Chem.*, 2015, **13** , 1983 - 1987 [Search PubMed] .

22. H. Shao , T. Nguyen , N. C. Romano , D. A. Modarelli and J. R. Parquette , *J. Am. Chem. Soc.*, 2009, **131** , 16374 -16376 CrossRef PubMed .
23. M. Yilmaz , M. Ozdemir , H. Erdogan , U. Tamer , U. Sen , A. Facchetti , H. Usta and G. Demirel , *Adv. Funct. Mater.*, 2015, **25** , 5669 -5676 CrossRef .
24. M. A. Khalily , G. Gulseren , A. B. Tekinay and M. O. Guler , *Bioconjugate Chem.*, 2015, **26** , 2371 -2375 CrossRef PubMed .
25. Y. X. Liu , Z. J. Du , Y. Li , C. Zhang , C. J. Li , X. P. Yang and H. Q. Li , *J. Polym. Sci., Part A: Polym. Chem.*, 2006,**44** , 6880 -6887 CrossRef .
26. F. Khelifa , S. Ershov , Y. Habibi , R. Snyders and P. Dubois , *ACS Appl. Mater. Interfaces*, 2013, **5** , 11569 -11577 Search PubMed .
27. I. Bressler , J. Kohlbrecher and A. F. Thunemann , *J. Appl. Crystallogr.*, 2015, **48** , 1587 -1598 Search PubMed .
28. I. Arioz , O. Erol , G. Bakan , F. B. Dikecoglu , A. E. Topal , M. Urel , A. Dana , A. B. Tekinay and M. O. Guler , *ACS Appl. Mater. Interfaces*, 2018, **10** , 308 -317 Search PubMed .
29. E. H. Rhoderick *IEE Proc., Part I: Solid-State Electron Devices*, 1982, **129** , 1 -14 CrossRef .
30. Y. K. Che , A. Datar , K. Balakrishnan and L. Zang , *J. Am. Chem. Soc.*, 2007, **129** , 7234 -7235 CrossRefPubMed .
31. T. Kitamura , S. Nakaso , N. Mizoshita , Y. Tochigi , T. Shimomura , M. Moriyama , K. Ito and T. Kato , *J. Am. Chem. Soc.*, 2005, **127** , 14769 -14775 CrossRef PubMed .
32. S. K. M. Nalluri , N. Shivarova , A. L. Kanibolotsky , M. Zelzer , S. Gupta , P. W. J. M. Frederix , P. J. Skabara , H. Gleskova and R. V. Ulijn , *Langmuir*, 2014, **30** , 12429 -12437 CrossRef PubMed .
33. X. Sun , G. Q. Lai , Z. F. Li , Y. W. Ma , X. Yuan , Y. J. Shen and C. Y. Wang , *Beilstein J. Org. Chem.*, 2015, **11** , 2343 -2349 CrossRef PubMed .
34. N. Amdursky , X. H. Wang , P. Meredith , D. D. C. Bradley and M. M. Stevens , *Adv. Mater.*, 2016, **28** , 2692 -2698 CrossRef PubMed .
35. M. Amit , S. Appel , R. Cohen , G. Cheng , I. W. Hamley and N. Ashkenasy , *Adv. Funct. Mater.*, 2014, **24** , 5873 -5880 CrossRef .
36. D. D. Ordinario , L. Phan , W. G. Walkup , J. M. Jocson , E. Karshalev , N. Husken and A. A. Gorodetsky , *Nat. Chem.*, 2014, **6** , 597 -603 CrossRef PubMed .
37. O. Silberbush , M. Amit , S. Roy and N. Ashkenasy , *Adv. Funct. Mater.*, 2017, **27** , 1604624 CrossRef .
38. S. Cukierman *Biochim. Biophys. Acta*, 2006, **1757** , 876 -885 CrossRef PubMed .